Geometry-Induced Rigidity in Nonspherical Pressurized Elastic Shells

A. Lazarus, H. C. B. Florijn, and P. M. Reis*

EGS. Lab: Elasticity, Geometry and Statistics Laboratory, Department of Mechanical Engineering, Department of Civil & Environmental Engineering, Massachusetts Institute of Technology, Cambridge, Massachusetts 02139, USA

(Received 16 July 2012; published 5 October 2012)

We present results from an experimental investigation of the indentation of nonspherical pressurized elastic shells with a positive Gauss curvature. A predictive framework is proposed that rationalizes the dependence of the local rigidity of an indented shell on the curvature in the neighborhood of the locus of indentation, the in-out pressure differential, and the material properties. In our approach, we combine classic theory for spherical shells with recent analytical developments for the pressurized case, and proceed, for the most part, by analogy, guided by our own experiments. By way of example, our results elucidate why an eggshell is significantly stiffer when compressed along its major axis, as compared to doing so along its minor axis. The prominence of geometry in this class of problems points to the relevance and applicability of our findings over a wide range of length scales.

DOI: 10.1103/PhysRevLett.109.144301 PACS numbers: 46.70.De, 81.70.Bt, 87.64.Dz

Shells are ubiquitous as both natural and engineered structures, including viral capsids [1], pollen grains, colloidosomes [2], pharmaceutical capsules, exoskeletons, mammalian skulls [3], pressure vessels, and architectural domes. In addition to their aesthetically appealing form, shells offer outstanding structural performance. As such, they typically have the function of enclosure, containment, and protection, with an eggshell being the archetypal example [Fig. 1(a)]. The mechanics of thin elastic shells [4,5] have long been known to be rooted in the purely geometric isometric deformations of the underlying curved surface, since stretching is energetically more costly than bending [6]. However, despite a vast literature on the isometry of rigid surfaces [7,8], establishing a general direct theoretical connection between the differential geometry of surfaces and the mechanics of shells is a challenging endeavor. This is due to the difficulties in systematically quantifying the effect of a small but finite thickness on the mechanical response of a curved surface. To circumnavigate this issue, explicit boundary value problem calculations tend to be performed by deriving the local equilibrium equations of 3D continuum mechanics and then taking the limit of a small but finite thickness within the kinematics [9]. For example, closed analytical solutions have been obtained in this fashion for the indentation of *spherical* unpressurized [10,11] and pressurized [12] shells. For more intricate geometries and mechanical environments, numerical methods can be used such as full scale finite element simulations [13,14]. Although powerful, these computational approaches can sometimes come at the detriment of physical insight and predictive understanding of the interplay between the mechanics of the structure and the geometry of its surface.

Here, we study the effect of the geometry of surfaces with a positive Gauss curvature on the linear mechanical response under the indentation of thin elastic shells, with or without an in-out pressure differential. Our goal is to quantify the geometry-induced rigidity (GIR) which we define as the amount by which a nonspherical shell is stiffened when compared to a spherical shell with the same thickness and material properties [15]. For this purpose, we perform precision desktop-scale experiments where both the geometry of the shells and their material properties are accurately custom controlled using rapid prototyping and digital fabrication techniques. The rigidity is quantified through indentation tests and the differential pressure is set by a syringe-pump system under feedback control. First, we study the rigidity at the pole of ellipsoidal shells with different aspect ratios toward investigating the

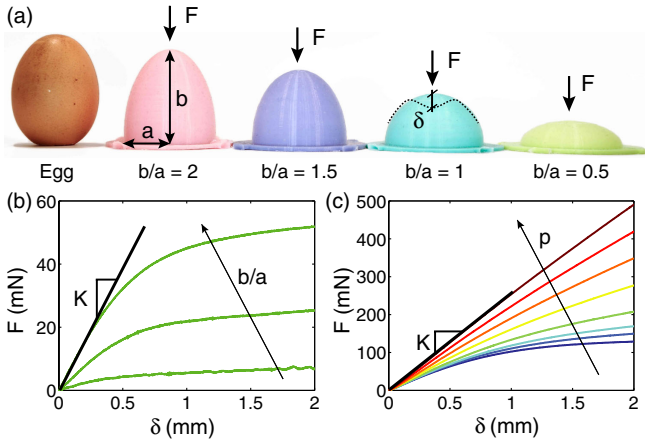

FIG. 1 (color online). (a) A chicken's egg and 500 μm thick ellipsoidal shell samples with four aspect ratios $b/a = \{2, 1.5, 1, 0.5\}$ and four elastomers with Young's modulus $E = \{0.2, 0.5, 0.6, 1\}$ MPa. (b) Load-displacement curves for indentation at the pole for an in-out differential pressure $p = 0$ Pa, $E = 1$ MPa, and three different aspect ratios $b/a = 0.5$, 1, and 2. (c) Load-displacement curves for indentation at the pole for $b/a = 1.5$, $E = 1$ MPa, and $0 < p < 10$ kPa.

specific case of axisymmetric convex surfaces. We then turn to ellipsoids indented along their meridian, where the surface has two distinct principal curvatures. Combining our experimental results with the classic theory of elasticity of spherical shells due to Reissner [10] as well as more recent developments by Vella *et al.* [12], we find that the effective rigidity is induced by (i) the local curvature in the neighborhood of the locus of indentation, (ii) the material properties of the shell, and (iii) the in-out differential pressure.

Fabricating our thin shells involves the conception of a computer assisted design model for a mold of the target shell structure, which is then 3D printed out of ABS plastic, and used to cast samples with Vinylpolysiloxane (a silicone-based elastomer). In our experiments, we use elastomers with four values of the Young's modulus in the range $0.2 < E < 1$ MPa and a Poisson ratio of $\nu \approx 0.5$. Inspired by the eggshell geometry [Fig. 1(a)], we print molds with four ellipsoidal shapes that set the geometric parameters to be four polar radii, $b = \{1.25, 2.5, 3.75, 5\}$ cm, an equatorial circular radius, $a = 2.5$ cm, and a thickness $t = 0.5$ mm (the latter two parameters are set constant for all experiments). This value of thickness ($t/a = 0.02 \ll 1$) ensures the validity of the thin shell assumption. In Fig. 1(a), we show photographs of four representative samples made of different polymers (different colors correspond to different values of E) with aspect ratios $b/a = \{0.5, 1, 1.5, 2\}$.

We start by vertically indenting the pole of unpressurized shell specimens using a hemispherical cap indentor (1.5 mm radius) at the constant speed of 1 mm/min, ensuring point indentation under quasistatic conditions. The compressive force F resulting from the indentation by the imposed displacement δ is recorded using the load cell of an Instron machine with a resolution of ± 100 μN. Typical load-displacement curves for shells with different aspect ratios are presented in Fig. 1(b). We focus on the first linear regime occurring for $\delta/t < 1$ and define the experimental rigidity K as the initial slope in the load-displacement curves. For a given material and shell thickness, the rigidity increases with the aspect ratio, suggesting the possibility of enhancing the rigidity of a thin elastic shell by simply changing its geometry.

To investigate this GIR behavior observed in Fig. 1(b), we now measure K at the pole for 16 unpressurized shell specimens (four aspect ratios b/a and four values of E). We quantify the GIR as the dimensionless ratio K/K_s where K_s is the theoretical rigidity of unpressurized *spherical* shells under indentation defined by Reissner [10] as $K_s = 8D/L_b^2$. Here, $D = Et^3/12(1-\nu^2)$ is the bending modulus of the shell, $L_b = (Da^2/Et)^{1/4}$ is a characteristic length scale arising from the balance of bending and stretching, and a is the radius chosen for reference. In Fig. 2(b), we present the dependence of the GIR at the pole on the shell's aspect ratio, finding that it scales proportional to b/a; i.e., for a given material, an ellipsoidal shell that is twice as high as the spherical counterpart is also twice as rigid.

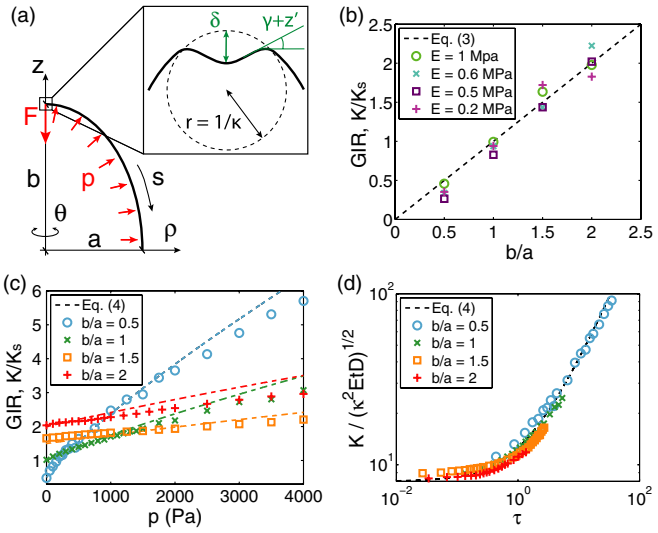

FIG. 2 (color online). Indentation at the pole. (a) Schematic of a deformed ellipsoidal specimen. (b) Dependence of GIR K/K_s on b/a for four different elastic polymers and $p = 0$. (c) GIR K/K_s, as a function of the internal pressure p for four aspect ratios $b/a = \{0.5, 1, 1.5, 2\}$ and $E = 1$ MPa. (d) Dimensionless experimental rigidity Kl_b^2/D against dimensionless pressure τ.

We rationalize the above observation by considering the equations for static equilibrium of thin elastic shells of revolution under indentation [5] and computing the mechanical stresses at the pole. In its stress-free reference configuration, the shell can be represented by the generating planar curves $\rho = \rho(s)$ and $z = z(s)$, where s is the arc-length along the shell's midplane [see the schematic diagram in Fig. 2(a)]. In order to understand the linear mechanical response, we consider the particular case of small strains and small rotations under indentation at the convex pole. Assuming axisymmetric and twistless deformations, the linear equilibrium equations can be written in the radial and axial directions, in term of s alone, as

$$\frac{d}{ds}(\rho\sigma_s\rho') - \sigma_\theta = 0, \tag{1}$$

$$\frac{1}{\rho}\frac{d}{ds}(\rho\sigma_s z') - \frac{D}{\rho}\frac{d}{ds}\left((\rho\gamma')' - \frac{\gamma}{\rho}\right) = -f_z, \tag{2}$$

where $\gamma(s)$ is the rotation angle between the reference and deformed configuration, $\sigma_s(s)$ and $\sigma_\theta(s)$ are the axial and hoop stresses, respectively, $f_z(s)$ is the force density per unit area in the axial direction, and $()'$ denotes differentiation with respect to s. For our particular ellipsoidal geometries, the generating planar curve is parametrized by $z(s) = b\sqrt{1-\rho^2(s)/a^2}$. In the neighborhood of the indentation point at the flat pole of the ellipsoid, where the deformations occur, the local generating plane curve can be described by the linear approximations $\rho(s) \approx s$,

$\rho'(s) \approx 1$, and $z'(s) \approx -s/r$, where $r = a^2/b$ is the local radius of curvature. For $s \ll r$, the angle $\gamma(s) + z'(s)$ [Fig. 2(a)] which measures the direction of the tangent along a deformed meridian, must vanish since this tangent is perpendicular to the pushing vertical indentor and $\gamma(s) = -z'(s) = s/r$. Replacing this local kinematics into the equilibrium equations (1) and (2), we find that the membrane stresses are given by $\sigma(s) \backsim E\kappa\delta(s)$ and therefore proportional to the local curvature at the pole, $\kappa = 1/r = b/a^2$ (the two principal curvatures are equal due to axisymmetry, $\kappa = \kappa_1 = \kappa_2$). After substituting the global natural bending length scale L_b introduced earlier by its local counterpart, $l_b = (D/Et\kappa^2)^{1/4}$, into K_s, we can generalize Reissner's rigidity at the pole of nonspherical thin elastic shells of revolution:

$$K_t^0 = \frac{4Et^2}{\sqrt{3(1-\nu^2)}}\kappa. \tag{3}$$

In particular, for an ellipsoidal shell where $\kappa = b/a^2$, we find that $K_t^0 = (b/a)K_s$, which is in excellent agreement with the experimental GIR data as a function of aspect ratios b/a presented in Fig. 2(b).

Having rationalized our results for unpressurized shells, we now investigate the influence of an in-out differential pressure on the rigidity of nonspherical axisymmetric shells. We focus on four elastomeric ellipsoidal shells with aspect ratios $b/a = \{0.5, 1, 1.5, 2\}$ and $E = 1$ MPa, and measure the rigidity K at their pole for differential pressures in the range $0 < p < 4$ kPa. Typical load-displacement curves for increasing p are shown in Fig. 1(c) for a shell with $b/a = 1.5$. The corresponding dependence of the GIR (K/K_s), on p is presented in Fig. 2(c) and we find that both pressure and geometry can enhance the rigidity. Above, we showed for the unpressurized case that the coupling between geometry and the mechanical response was dictated by the local curvature. This now motivates us to proceed by hypothesizing that the local nature of the GIR also translates into the pressurized case. If this hypothesis is correct, we should therefore find that the indentation at the pole of a pressurized ellipsoidal shell is locally identical to the indentation of a pressurized spherical shell of radius $r = 1/\kappa = a^2/b$. As such, we seek a generalization of the theoretical rigidity of the pressurized spherical shell of Vella *et al.* [12],

$$K_t^p = \frac{8D}{l_b^2}\frac{\pi(\tau^2-1)^{1/2}}{2\,\mathrm{arctanh}(1-\tau^{-2})^{1/2}}, \tag{4}$$

where we replace a by the local radius of the curvature at the pole $r = 1/\kappa$, where $\kappa = \kappa_1 = \kappa_2$, so that $\tau = pr^2/4(EDt)^{-1/2}$ is a local dimensionless internal pressure and l_b is the local bending scale at the pole defined above. The dependence of the dimensionless experimental rigidity, Kl_b^2/D, on the local dimensionless pressure τ is showed in Fig. 2(d), where we find that all the experimental data collapse onto the predicted rigidity K_t^p (dashed line). This excellent agreement confirms that Eq. (4) accurately captures the experimental rigidity at the pole of pressurized thin ellipsoidal shells, which corroborates our hypothesis.

We progress by generalizing the current framework to nonaxisymmetric convex shells which are locally characterized by two distinct principal curvatures κ_1 and κ_2, a Gauss curvature $\kappa_G = \kappa_1\kappa_2$, which we restrict to be positive, and a mean curvature $\kappa_M = (\kappa_1 + \kappa_2)/2$ [Fig. 3(a)]. For the moderately elongated ellipsoids we consider in our study, $\kappa_M \approx \sqrt{\kappa_G}$, as shown in Fig. 3(b), with representative schematics in the inset. Encouraged by our previous success in characterizing the rigidity of convex axisymmetric shells, we proceed again by analogy and hypothesize that the local mean curvature κ_M generalizes the role of κ in the GIR of nonaxisymmetric shell surfaces. Note that, as required, this generalization reduces to $\kappa_M = \kappa_1 = \kappa_2 = \kappa$ at the pole. Thus, replacing $\kappa = 1/r$ by κ_M in Eqs. (3) and (4), we propose a combined expression that describes the rigidity of unpressurized or pressurized nonspherical shells with a positive Gauss curvature,

$$K_t = \frac{4Et^2}{\sqrt{3(1-\nu^2)}}\kappa_M\frac{\pi/2(\tau^2-1)^{1/2}}{\mathrm{arctanh}(1-\tau^{-2})^{1/2}}, \tag{5}$$

where τ is the local dimensionless pressure introduced above with $r = 1/\kappa_M$.

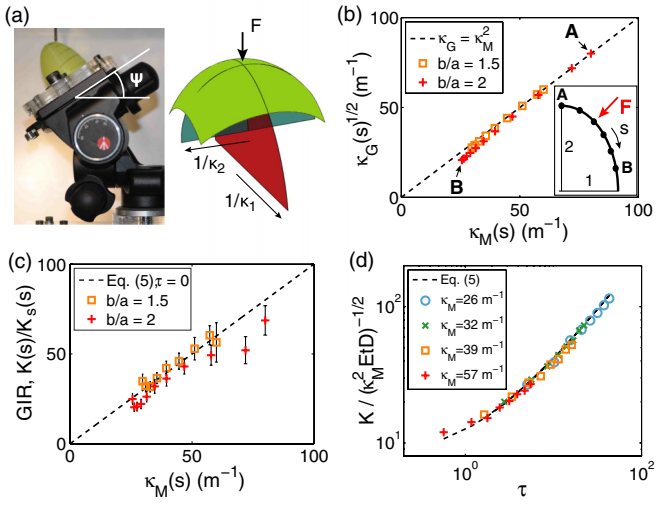

FIG. 3 (color online). (a) Experimental setup for shells with two distinct principal curvatures κ_1 and κ_2. (b) Evolution of the Gauss and mean curvatures along the meridian of the ellipsoids with $b/a = 1.5$ and 2. (c) Evolution of geometry-induced rigidity $K/K_s(s)$ with mean curvature $\kappa_M(s)$ for two unpressurized shells with aspect ratios $b/a = 1.5, 2$ and $E = 1$ MPa. (d) Evolution of dimensionless experimental rigidity $K(s)l_b^2(s)/D(s)$ with dimensionless pressure τ for four points along the meridian of a pressurized shell with $b/a = 2$ and $E = 1$ MPa.

A modification of our experimental setup that allows for indentation in regions with two different principal curvatures, κ_1 and κ_2, is now used to test the proposed Eq. (5). For this, two shells with Young's modulus $E = 1$ MPa and aspect ratios $b/a = 1.5$ and 2 are marked every $s_i = 0.5$ cm along one meridian from the pole to the base [Fig. 3(a)]. Once pressurized to a set constant p, the shells are indented at the points $P(s_i)$ with the compressive force F aligned perpendicularly to the surface. For a given differential pressure p, we measure the experimental local mean curvature $\kappa_M(s_i)$ using digital image processing at each indentation point $P(s_i)$ along the meridian of our shell specimen [Fig. 3(b)].

In Fig. 3(c), we plot the dependence of the Geometry-Induced Rigidity, $K(s_i)/K_s(s_i)$, on the mean curvature $\kappa_M(s_i)$ for two unpressurized shells with aspect ratios $b/a = 1.5$ and 2 [Reissner's result per unit radius $K_s(s_i) = 4Et(s_i)^2/\sqrt{3(1-\nu^2)}$ is used as the reference rigidity $K_s(s_i)$]. As expected, the measured $K(s_i)$ scales linearly with Reissner's rigidity $K_s(s_i)$ with a prefactor $\kappa_M(s_i)$, i.e., $K(s_i) = \kappa_M(s_i)K_s(s_i)$, which conforms to Eq. (5) with a dimensionless differential pressure $\tau = 0$. The role of κ_M in moderately nonaxisymmetric shells also extends to the pressurized case, as shown in Fig. 3(d), where we plot the evolution of dimensionless experimental rigidities $K(s)l_b(s)^2/D$ as a function of dimensionless pressure $\tau(s)$ for four indentation points $P(s_i)$ along the shell with $b/a = 2$. We find excellent agreement between the experimental rigidities $K(s_i)$ and the predicted $K_t(s_i)$ (dashed line) confirming the accuracy of Eq. (5).

Having learned about the geometry-induced rigidity in convex elastic shells through Eq. (5), we turn our learnings into an inverse problem toward developing a nondestructive method to measure the parameters of the shell (e.g., shell thickness) upon knowing the geometry of the underlying surface and the local mechanical response. Fortunately, the thickness profile of our experimental samples varied slightly along the meridian of our shells due to limitations of our fabrication procedure; the male and female parts of the molds were not perfectly aligned during casting. Earlier, when we tested Eqs. (3)–(5), we took for the thickness, $t(s_i)$, the local average measured over a curvilinear distance $s = 3 \times l_b$ in the neighborhood of the indentation point $P(s_i)$ obtained by cutting the shell in half and analyzing the profile with a digital flat scanner [Fig. 4 (inset)]. Note that in our experiments, the local bending scale, $1.6 < l_b = (D/Et\kappa_M^2)^{1/4} < 2.5$ mm, is of the order of the diameter of the hemispherical cap indentor $\Phi = 3$ mm. In Fig. 4, we compare this average thickness $t(s_i)$ along the meridian of two shell specimens measured directly from the scanned profiles of the cut shells, with the thickness predicted from Eq. (5) with $\tau = 0$, through indentation. The variation of the thickness profile is accurately captured within a spatial resolution of $s \approx 2l_b \approx 5$ mm, confirming the relevance of the local bending scale

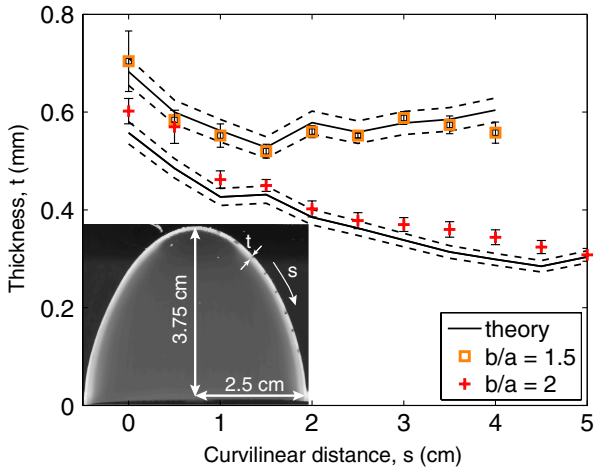

FIG. 4 (color online). Comparison between measured and predicted thickness profile for two unpressurized shells with $b/a = 1.5$ and 2 and $0.9 < E < 1$ MPa. Solid and dashed lines represent mean value ± standard deviation for the predicted thickness. (Inset) Scanned image of a shell with aspect ratio $b/a = 1.5$ cut in half.

l_b as a measure of locality. More importantly, the fact that we are able to recover the thickness profile using Eq. (5) demonstrates that our proposed description can be used as a precision nondestructive technique for nonspherical thin elastic shell with a positive Gauss curvature.

In summary, we have quantified the relation between geometry and the mechanical rigidity of positively curved thin elastic shells under pressure, arriving to our predictive framework primarily by analogy and an analysis of precision experimental data. Our work calls for a formal identification, in particular, for a higher degree of asphericity $\epsilon = (\kappa_2 - \kappa_1)/(\kappa_2 + \kappa_1)$, where our description is likely to be challenged, which will require a theoretical effort that we hope our work will help catalyze. Still, the range of curvatures we have considered ($0 < \epsilon < 0.6$ for which $\kappa_M \approx \sqrt{\kappa_G}$), is applicable and relevant across a wide range of practical instances of natural and man-made nonspherical shells. The scale invariance of geometry-induced rigidity suggests that our framework should find uses across length scales: from the mechanical testing of viral capsids through atomic force microscopy [16], to ocular tonometry procedures [17] or in the design of architectural shells [18]. Moreover, one can now interpret the increased stiffness of a chicken egg compressed along its poles as compared to doing so along the equator as being attributed to geometry-induced rigidity.

We thank C. Perdigou for help with preliminary experiments and B. Audoly, D. Vella, A. Vaziri, and A. Boudaoud for enlightening discussions.

Note added.—During the preparation of our manuscript, we became aware of the complementary theoretical and numerical work of D. Vella *et al.* [19], on a similar topic.

*To whom correspondence should be addressed.
preis@mit.edu

[1] T. Baker, N. Olson, and S. Fuller, Microbiol. Mol. Biol. Rev. **63**, 862 (1999).
[2] A. Dinsmore, M. Hsu, M. Nikolaides, M. Marquez, A. Bausch, and D. Weitz, Science **298**, 1006 (2002).
[3] D. Hu, K. Sielert, and M. Gordon, J. Mech. of Mater. and Struct. **6**, 1197 (2011).
[4] G. Wempner and D. Talaslidis, *Mechanics of Solids and Shells* (CRC press, Boca Raton, FL, 2003).
[5] B. Audoly and Y. Pomeau, *Elasticity and Geometry: From Hair Curls to the Nonlinear Response of Shells* (Oxford press, New York, 2010).
[6] J. H. Jellett, Trans. R. Irish Acad. **22**, 343 (1849); J. Rayleigh, *The Theory of Sound* (Dover Publications, New York, 1976), Vol. 1.
[7] A. Pogorelov, *Extrinsic Geometry of Convex Surfaces* (American Mathematical Society, Providence, RI, 1988).
[8] I. Ivanova-Karatopraklieva and I. Sabitov, J. Math. Sci. Univ. Tokyo **74**, 997 (1995).
[9] A. E. H. Love, *A Treatise on the Mathematical Theory of Elasticity* (Dover Publications, New York, 1944); A. Goldenveizer, *Theory of Elastic Thin Shells* (Pergamon Press, New York, 1961); F. Niordson, *Shell Theory*, North-Holland Series in Applied Mathematics and Mechanics (North Holland, New York, 1985).
[10] E. Reissner, J. Math. Phys. (Cambridge, Mass.) **25**, 80 (1946); **25**, 279 (1946).
[11] A. Pogorelov, *Bending of Surfaces and Stability of Shells* (American Mathematical Society, Providence, RI, 1988).
[12] D. Vella, A. Adjari, A. Vaziri, and A. Boudaoud, J. R. Soc. Interface **9**, 448 (2012).
[13] D. Chapelle and K.-J. Bathe, *The Finite Element Analysis of Shells: Fundamentals* (Springer, New York, 2010).
[14] A. Vaziri and L. Mahadevan, Proc. Natl. Acad. Sci. U.S.A. **105**, 7913 (2008); A. Vaziri, Thin-Walled Struct. **47**, 692 (2009).
[15] Note that our notion of *GIR* in thin shells is not to be confused with the established concept of *geometric stiffening* which is a stiffening (or weakening), typically also for a thin structure, due to a varying stress state as explained in R. Levy and W. R. Spillers, *Analysis of Geometrically Nonlinear Structures* (Kluwer Academic Publishers, Dordrecht, 2003).
[16] M. Arnoldi, M. Fritz, E. Bäuerlein, M. Radmacher, E. Sackmann, and A. Boulbitch, Phys. Rev. E **62**, 1034 (2000); I. Ivanovska, G. Wuite, B. Jönsson, and A. Evilevitch, Proc. Natl. Acad. Sci. U.S.A. **104**, 9603 (2007); W. Roos and G. J. L. Wuite, Adv. Mater. **21**, 1187 (2009); W. Roos, R. Bruinsma, and G. Wuite, Nature Phys. **6**, 733 (2010).
[17] S.-Y. Woo, A. S. Kobayashi, C. Lawrence, and W. A. Schlegel, Ann. Biomed. Eng. **1**, 87 (1972); A. Elsheikh, D. Wang, A. Kotecha, M. Brown, and D. Garway-Heath, Ann. Biomed. Eng. **34**, 1628 (2006).
[18] H.-J. Schock, *Soft Shells: Design and Technology of Tensile Architecture* (Birkhäuser, Basel, 1997); C. Ceccato, L. Hesselgren, M. Pauly, H. Pottmann, and J. Wallner, *Advances in Architectural Geometry 2010* (Springer Wien, New York, 2010).
[19] D. Vella, A. Adjari, A. Vaziri, and A. Boudaoud, Phys. Rev. Lett. **109**, 144302 (2012).